Unveiling Dusty Starbursts by ngVLA Observations of Radio Recombination Lines

Tomonari Michiyama[1], Kouichiro Nakanishi[2], Daisuke Iono[2]

[1]*Kavli Institute for Astronomy and Astrophysics, Peking University, 5 Yiheyuan Road, Haidian District, Beijing 100871, P.R.China*

[2]*National Astoronomical Observatory of Japan, 2–21–1 Osawa, Mitaka-shi, Tokyo 181–8588*

t.michiyama.astr@gmail.com

Abstract

The observation of radio recombination lines (RRLs) is one of the most powerful tools to investigate extremely dusty starburst activities in nearby galaxies because RRLs are extinction free direct probes of ionizing photons that are produced by young massive stars. The benefit of sensitive observations with high angular resolution of RRLs by ngVLA are as follows, we can (1) identify dusty starburst regions where optical observations such as Hα and Hβ are not detected, (2) constrain the timescale of starbursts, (3) measure the properties of H$\textsc{ii}$ regions (i.e., electron temperature). The ngVLA will detect $\sim 1-10$ pc scale star forming clumps (with a SFR of ~ 0.02 $M_\odot$ yr^{-1}) in a central molecular zone of active galaxies such as luminous infrared galaxies that often have extremely dusty starburst regions (e.g., NGC 3256 at 40 Mpc) as well as the Milky Way and nearby starburst galaxies (e.g., NGC 253 at 3 Mpc). This project can answer whether the star formation process on $\sim 1-10$ pc scale clumps is uniform in normal star forming and extreme starburst galaxies or not.

Key words: starburst galaxy — radio recombination line — U/LIRG

1. Introduction

For 13.8 billion years after the big bang, individual galaxies have formed stars with unique histories that depend on e.g., their mass, morphology, and environment. One of the most important achievements of past years is mapping the history of star formation in the universe. Madau et al. (1996) show that the galaxies were more actively forming stars at $z \sim 2-3$ (called Cosmic Noon), suggesting that a significant fraction of stars formed in short episodic events. This implies that the number of galaxies that are experiencing a period of intense star formation called "starburst galaxies" are common at Cosmic Noon. The open question is that "How are starbursts triggered and regulated?". In order to answer this question, it is necessary to link star formation processes on small scale clouds with the size of $1-10$ pc and global galaxy properties. For this purpose, the immediate issue that ngVLA can challenge is measuring the properties of $1-10$ pc clumps in very active galaxies. The goal of our proposing ngVLA science is to answer whether the star formation process on a small scale is uniform in normal star forming and extreme starburst galaxies or not.

The most important parameter to explain starburst activities is the number of newborn stars per year, called star formation rate (SFR in the unit of $M_\odot$ yr^{-1}). In the case of the Milky Way, SFR is measured for 0.68-1.45 $M_\odot$ yr^{-1} by counting the number of young stellar objects (YSOs) through e.g., Spitzer/IRAC survey of the Galactic plane (Robitaille & Whitney 2010). Besides, SFR = 0.08 $M_\odot$ yr^{-1} is measured in the central molecular zone (CMZ) of the Milky Way (Immer et al. 2012), where CMZ is the central 100×500 pc^2 region.

In the case of other galaxies, it is impossible to directly count the number of YSOs. Instead, we can predict SFR from the number of UV photons that are produced by YSOs in galaxies. We can also use hydrogen recombination lines such as Hα and Hβ because YSOs ionize gas around. However, interstellar dust often veils the information of UV photons and optical lines in intense starburst galaxies. When we measure SFR in dusty starburst galaxies, we often use infrared (IR) luminosity because interstellar dust absorbs starlight and re-emits it in the IR. The details on the SFR measurements are reviewed by e.g., Kennicutt & Evans (2012); Calzetti et al. (2012).

Using these techniques, astronomers found nearby starburst galaxies that are the main targets in this project. Especially, infrared method is important to find starburst galaxies. For example, in the case of one galaxy NGC 253, SFR = 3.5 $M_\odot$ yr^{-1} in CMZ (Melo et al. 2002), suggesting ten times more intense star formation activities than CMZ of the Milky Way. Therefore, NGC 253 is referred to as a starburst galaxy. One of the most important achievements by infrared telescopes such as Infrared Astronomical Satellite (IRAS) is the discovery of luminous infrared galaxies (LIRGs: 10^{11} $L_\odot < L_{\rm FIR} < 10^{12}$ $L_\odot$) and ultra-luminous infrared galaxies (ULIRGs: 10^{12} $L_\odot < L_{\rm FIR} < 10^{13}$ $L_\odot$) whose SFR is 10-1000 $M_\odot$ yr^{-1}. It is said that dust obscured star formation activities (e.g., in U/LIRGs) dominate the star formation budget at Cosmic Noon (Zavala et al. 2021).

The main goal of this project is to comprehensively understand the star formation process in normal star forming galaxies like the Milky Way and intense dusty starburst galaxies like U/LIRGs, i.e., how to trigger and quench starbursts. In order to achieve this goal, it is necessary to access a small scale because the global SFR in galaxies is determined by the ensemble of each star forming clouds. However, UV and optical telescopes are not powerful in this purpose due to dust extinction. While infrared telescopes are very powerful to identify dusty starburst galaxies, it is difficult to achieve higher angular resolution (than optical telescopes and radio interferometers) due to diffraction limits. Therefore, radio (including millimeter) interferometers are important for our study.

One of the most powerful methods to investigate dusty in-

tense starbursts is hydrogen radio recombination lines (RRLs) because RRLs are extinction free direct probes of ionizing photons that are produced by young massive stars. Since RRLs are faint (e.g., 0.05 times fainter than Hydrogen cyanide (HCN) for RRLs at ∼100 GHz), only tentative detections in nearby galaxies were achieved by VLA so far (Section 2.1). Now, Atacama Large Millimeter/submillimeter Array (ALMA) can detect RRLs in high signal to noise ratio in nearby galaxies (Section 2.2). However, ALMA cannot investigate the very active galaxies such as U/LIRGs that are in a relatively distant universe due to angular resolution and sensitivity limits. Therefore, ngVLA is the only telescope to detect RRLs from ∼pc scale clumps in the CMZ of nearby active dusty galaxies such as U/LIRGs.

In Section 2, we briefly summarize the basic information and observations of RRLs in nearby galaxies by VLA and ALMA. In Section 3, we explain our targets (NGC 253 and NGC 3256). In Section 4, we explain the science goals. Section 5 is a summary of this article.

2. Basic information

2.1. What are RRLs?

Radio spectrometers enable us to observe spectral lines from various molecules and atoms. In this article, we focus on spectral lines emitted when electrons and ions combine. Except for the early universe, ionized gas is produced by the ionization of neutral atoms, so it is called "recombination" in the sense that these atoms recombine to return to neutral. Recombination lines have been observed in interstellar space, including hydrogen, helium, and carbon. In the case of hydrogen atoms, the Lyman series, which transitions to the energy level of principal quantum number $n = 1$, is emitted in the ultraviolet region, while the Balmer series, which transitions to the level of $n = 2$, is mainly emitted in the visible light region. But when n transitions to the tens of levels, it is emitted in the radio region and called radio recombination lines (RRLs). The frequency ν of the lines in these series can be represented by a simple formula of

$$\nu_{n_2 \to n_1} = Rc \left(\frac{1}{n_1{}^2} - \frac{1}{n_2{}^2} \right), \tag{1}$$

where n_1 and n_2 are positive integers ($n_2 > n_1 > 1 > 0$), c is the speed of light, and constant R is called as the Rydberg constant. For example, in the case of $n_1 = 40$ and $n_2 = 41$, the frequency is 99.0 GHz (represented as H40α). The lines that ngVLA can observe are shown in Figure 1. The ngVLA can observe RRLs that ALMA does not cover (e.g., $n \gtrsim 60$).

According to Gordon & Sorochenko (2002), the first detection of RRLs was succeeded by Pulkovo radio astronomers in 1964. They detected H104α at 5.76 GHz in the Omega and Orion nebula. In 1977, the detections of RRLs in extragalactic galaxies were reported e.g., in M82 (Shaver et al. 1977; Bell & Seaquist 1977; Chaisson & Rodriguez 1977) and NGC 253 (Seaquist & Bell 1977). In the 1990s, radio interferometers such as VLA and millimeter single dish telescopes such as Nobeyama (NRO45m) detected RRLs in other galaxies such as NGC 2146, NGC 1365, NGC 3638, IC694 NGC 3690, Arp 220, M83, and NGC 660 (see references in Gordon &
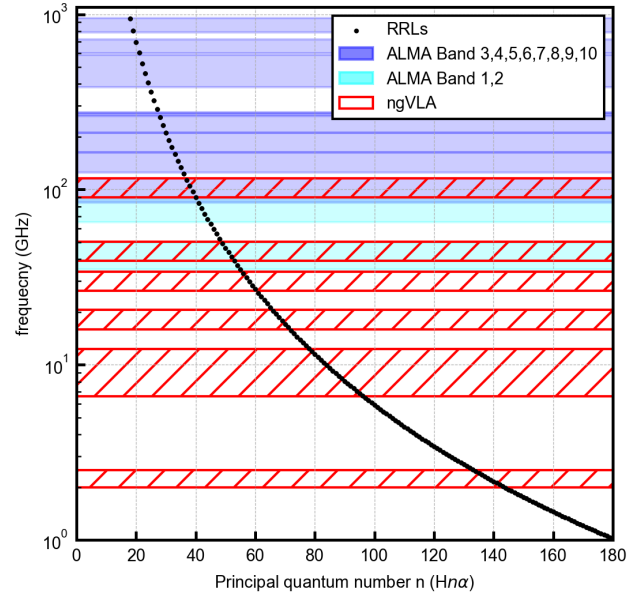

Fig. 1. The black dots indicate the frequency of H$n\alpha$ emission. The horizontal shades indicate the frequency coverage of ngVLA (red) and ALMA (blue for receivers in operation and cyan is for receivers in development). Thanks to the wide frequency coverage of ngVLA, we can observe RRLs in any receiver.

Sorochenko 2002). However, due to limited sensitivity and angular resolution, we cannot understand star formation processes in galaxies based on these observations.

2.2. Observations of RRLs by ALMA

In the ALMA era, RRLs are observed in various nearby galaxies, e.g., NGC 253 (Bendo et al. 2015), NGC 4945 (Bendo et al. 2016). These studies demonstrated that RRLs observations by ALMA are necessary to understand starburst activities at dusty regions ($A_V > 10$) by cross-checking SFR from RRLs and the other wavelengths. Recently Michiyama et al. (2020) observed RRLs to investigate dusty starbursts in a merging galaxy NGC 3256 which is a LIRG at relatively distant universe ($D_L \sim 40$ Mpc). In this galaxy, H40α and H42α were detected by ALMA, identifying nuclear starbursts where Hβ emissions are undetected due to dust extinction ($A_V \sim 25$) even by deep observations of Multi Unit Spectroscopic Explorer at the Very Large Telescope of the European Southern Observatory (MUSE). In the case of a nearby galaxy, ALMA identifies compact ($\sim$ a few pc) RRLs sources. For example, Emig et al. (2020) detected RRLs from compact sources with the sizes of 1.4-4.0 pc in NGC 4945 ($D_L = 3.8$ Mpc).

2.3. Conversion from hydrogen recombination lines to SFR

The SFR can be predicted by ionizing photon rate Q [s^{-1}]. For example,

$$\frac{\text{SFR}}{\text{M}_\odot \text{ yr}^{-1}} = 5.41 \times 10^{-54} \left[\frac{Q}{\text{s}^{-1}} \right] \tag{2}$$

is used, where the conversion coefficient depends on the shape and mass range of the initial mass function (IMF) of the stars, and timescale (τ) over which star formation needs to remain constant, and on stellar rotation effects (see Bendo et al. 2015 and Bendo et al. 2016, for more details). The ionizing photon rate Q [s^{-1}] can be estimated by

$$\frac{Q}{\text{s}^{-1}} = \left[\frac{\alpha_{\text{B}}}{\text{cm}^3 \text{ s}^{-1}}\right]\left[\frac{EM}{\text{cm}^{-3}}\right], \tag{3}$$

where α_{B} is the total recombination coefficient and emission measure (EM) is $n_{\text{e}}n_{\text{p}}V$ (n_{e}, n_{p}, and V are ionized electron volume density, proton volume density, and volume of ionized H $_{\text{II}}$ region), respectively. The EM can be predicted by recombination line luminosity (L_{RL})

$$\frac{EM}{\text{cm}^{-3}} = \left[\frac{L_{\text{RL}}}{\text{erg s}^{-1}}\right]\left[\frac{\epsilon}{\text{erg s}^{-1} \text{ cm}^{-3}}\right]^{-1}, \tag{4}$$

where ϵ is the emissivity per unit of $n_{\text{e}}n_{\text{p}}$. By using equation 2, 3, and 4, SFR can be estimated as

$$\frac{\text{SFR}_{\text{RL}}}{\text{M}_\odot \text{ yr}^{-1}} = 5.41 \times 10^{-54}$$
$$\times \left[\frac{\epsilon}{\text{erg s}^{-1} \text{ cm}^{-3}}\right]^{-1}\left[\frac{\alpha_{\text{B}}}{\text{cm}^3 \text{ s}^{-1}}\right]\left[\frac{L_{\text{RL}}}{\text{erg s}^{-1}}\right]. \tag{5}$$

The equations are based on Michiyama et al. (2020); Bendo et al. (2015); Bendo et al. (2016).

3. Request Observations

As shown in Section 1, CMZ is the place for massive star-formation and dusty intense starburst activities. The goal of this project is to answer "whether the star formation process is uniform in the CMZ of normal star forming and extreme starburst galaxies". The ngVLA can distinguish two possible scenarios to answer why global SFR in CMZ is different among galaxies as follows.

- The local star formation process is uniform among the tree galaxies. This suggests that the number of star forming regions is varied among galaxies.
- The properties of small clumps are different among the three, suggesting small scale star formation process is varied among galaxies.

In order to make the observation strategy, we choose CMZ in the Milky Way, NGC 253, and NGC 3256 as an example. Figure 2 is a summary of carbon monoxide (CO) and RRLs observations of these galaxies and Table 1 is a summary of the basic information.

In the case of CMZ of the Milky Way, single dish telescopes achieve $\sim$pc scale spatial resolution. For example, CO (1–0) survey by NRO45m achieves the angular resolution of $\sim 17''$ that corresponds to $\sim$0.7 pc. Jones et al. (2011) detected H51α−H58α emission at Sagittarius B2 (Sgr B2). Based on Figure 2(a3), the total integrated H51α intensity is 426 [K km s^{-1}], which corresponds to $L_{\text{H51}\alpha} = 5.7 \times 10^{31}$ [erg s^{-1}] within the aperture radius of $140''(\sim$ 6 pc). Assuming the electron temperature (T_{e}) of 5000 K and electron density (n_{e}) of 10^3 cm^{-3}, the expected SFR is

~ 0.01 $M_\odot$ yr^{-1}. We note that RRLs mapping of the entire CMZ is difficult by single dish even for the Milky Way (see Jones et al. 2012 and MALT90 project[1]). The RRLs mapping of the Milky Way CMZ should be also an important mission that single dish mode and compact array of ngVLA will complete.

In the CMZ of NGC 253, Bendo et al. (2015) identified three blobs i.e., C, W, E in Figure 2(b2), with the $\sim 1''8$ (~ 30 pc) resolution H40α map. The SFR is 0.63 ± 0.06, 0.29 ± 0.02, and 0.17 ± 0.02 $M_\odot$yr^{-1} for C, W, E, respectively. Although high angular resolution observations by VLA and ALMA have already demonstrated that detecting RRL in $\sim$pc scale is feasible (e.g., Mohan et al. 2005 for VLA; Nakanishi+ in prep. for ALMA), only small numbers of $\sim$pc scale star-forming clumps were detected due to the limited sensitivity. The ngVLA will enable us to identify many faint and small clumps that VLA and ALMA are missing.

In the case of merging starburst galaxy NGC 3256, H40α emission indicates that SFR is 9.8 ± 0.5 $M_\odot$ yr^{-1} and 6.8 ± 0.5 $M_\odot$ yr^{-1} at the northern and southern nucleus, respectively. The achieved angular resolution is $1.5''(\sim 300$ pc), which means that we can only access global SFR at CMZ in NGC 3256 (Michiyama et al. 2020). What ALMA told us is that the SFR in CMZ of NGC 3256 is ~ 10 times larger than CMZ of NGC 253 and ~ 100 times larger than CMZ of the Milky Way. This ALMA project demonstrated that only RRLs can investigate the starburst activities in extremely dusty regions. When we use ngVLA, we can observe RRLs at starburst clumps like SgrB2. For example, ngVLA can achieve 10 mas (~ 2 pc) resolution at H40α. Assuming 1h integration with the velocity resolution of 10 km s^{-1}, we can achieve the sensitivity of 42.3 μJy. This sensitivity corresponds 3σ upper limit of SFR=0.02 $M_\odot$ yr^{-1} assuming that velocity width of the clump is 30 km s^{-1}. This means that ngVLA can detect $1 - 10$ pc clumps like SgrB2 at NGC3256.

In summary, single dish telescopes detected RRLs at 1-10 pc clumps such as SgrB2, and ALMA has been detected same size clumps in very nearby starburst galaxy such as NGC 253, and ngVLA will detect the small clumps in extremely dusty regions such as CMZ of NGC 3256.

4. Expected Outcome

4.1. Gas depletion time scale of $1 - 10$ pc clumps

Thanks to the wide instantaneous bandwidth and the long baseline that ngVLA will provide, RRLs and molecular lines such as CO and HCN can be simultaneously observed with high angular resolution. This means that we can simultaneously access the information of both SFR and molecular gas mass (M_{H2}) of $1 - 10$ pc clumps. We can investigate the time scale in terms of gas depletion, called gas depletion time ($\tau_{\text{gas}} = M_{\text{H2}}/$SFR or $\Sigma_{M_{\text{H2}}}/\Sigma_{\text{SFR}}$, where $\Sigma_{M_{\text{H2}}}$ and Σ_{SFR} is the surface density of molecular gas and SFR). It is said that τ_{gas} is much longer in the normal star forming galaxies than active galaxies like U/LIRGs (Daddi et al. 2010). In most cases, especially in radio astronomy, the conversion factor (from CO luminosity to molecular gas mass) is highlighted when we in-
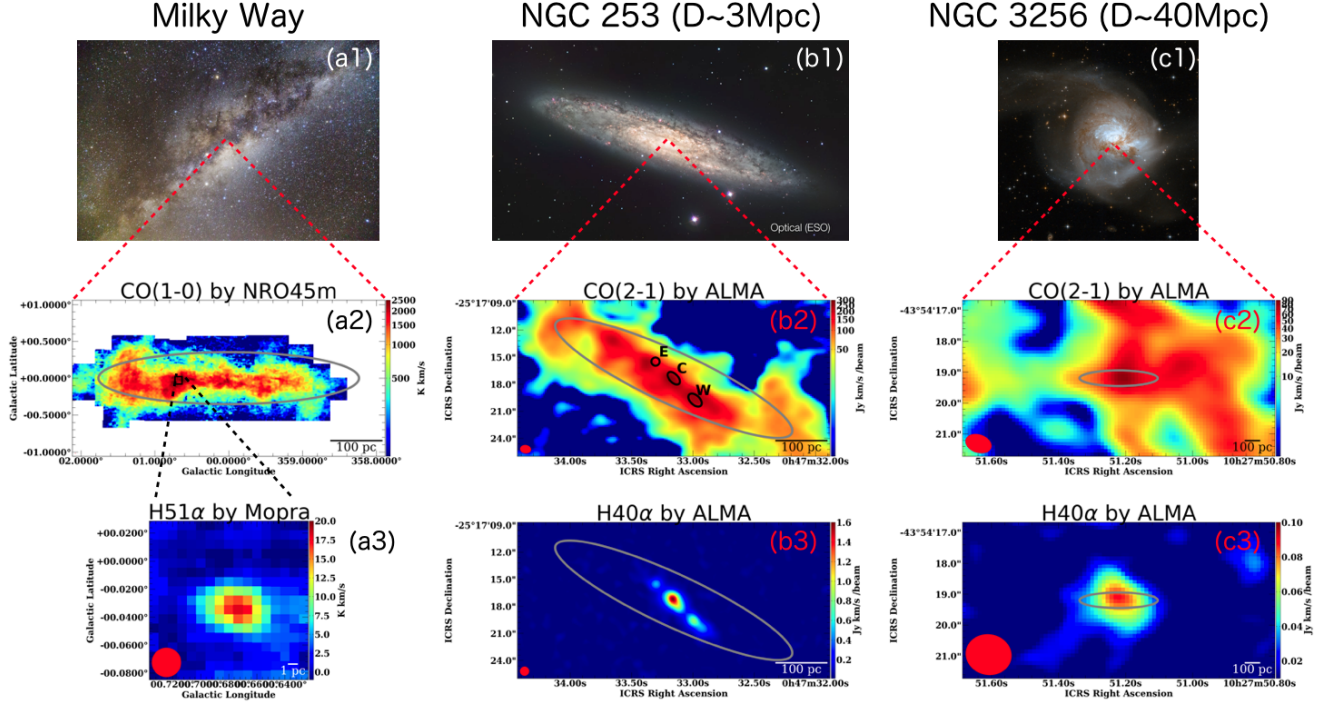
---
[1] http://malt90.bu.edu

Fig. 2. (a1) Night landscape photograph including Galactic center taken by Ko Hosokawa. (a2) CO (1–0) map of CMZ in the Milky Way obtained by NRO45m (Oka et al. 1998). The data was downloaded from NRO45m Data Release page https://www.nro.nao.ac.jp/~nro45mrt/html/results/data.html. The angular resolution is $17''(\sim 0.67$ pc). (a3) H58α map of SgrB2 obtained by Mopra (Jones et al. 2011). The data was downloaded from Mopra Central Molecular Zone Survey webpage https://atoa.atnf.csiro.au/CMZ. The angular resolution is $75''(\sim 3$ pc). (b1) Optical image of NGC 253 downloaded from NASA website (https://svs.gsfc.nasa.gov/30980). (b2) The CO (2–1) map of NGC 253 obtained by ALMA. The data was downloaded from Japanese Virtual Observatory (JVO, http://jvo.nao.ac.jp/portal/v2/) with the fits name of member.uid___A001_X1284_Xf59.ngc253_sci.spw29.cube.I.pbcor.fits. The black ellipticals indicates the region where H40α is detected. The angular resolution is $1''2 \times 0''9$ ($\sim 20 \times 16$ pc). (b3) The H40α map of NGC 253 obtained by ALMA (Nakanishi et al., in prep). The data was based on the project of 2016.1.00732.S. The angular size is smoothed in $1''(\sim 17$ pc). (c1) Optical image of NGC 3256 downloaded from ESA website (https://esahubble.org/images/heic0810ar/). (c2) The CO (2–1) map of NGC 3256 obtained by ALMA. The data was downloaded from JVO with the fits name of member.uid___A001_X2d6_Xb0.ari_l.NGC_3256_sci.spw0_227531MHz.12m.cube.I.pbcor.fits and member.uid___A001_X2d6_Xb0.ari_l.NGC_3256_sci.spw1_229289MHz.12m.cube.I.pbcor.fits. The angular resolution is $0''86 \times 0''59$ ($\sim 15 \times 10$ pc). The map is not entirely the full field of view (zooming up to the southern nucleus). (c3) The H40α map of NGC 3256 obtained by ALMA (Michiyama et al. 2020). The angular resolution is $1''5 \times 1''3$ ($\sim 26 \times 23$ pc). In each panel, the grey elliptical indicates the 500 pc $\times$ 100 pc CMZ region.

Name	D_{L}	1 pc	SFR$_{\mathrm{CMZ}}$ $M_\odot$ yr^{-1}	SFR$_{\mathrm{total}}$ $M_\odot$ yr^{-1}	$\Sigma_{\mathrm{SFR}}^{3\sigma}$ $M_\odot$ yr^{-1} pc^{-1}
(1)	(2)	(3)	(4)	(5)	(6)
Milky Way	8 kpc	$25''$	0.08	0.68-1.45	–
NGC 253	3 Mpc	58 mas	1.73±0.12	4.2	5.0e-06
NGC 3256	40 Mpc	5 mas	6.8±0.3	49±2	1.6e-04

Table 1. Information of Milky Way, NGC 253, and NGC 3256. (1) Name. (2) Distance. (3) The angular scale corresponding to 1 pc. (4) SFR in central molecular zone. The references are Immer et al. (2012), Melo et al. (2002), and Michiyama et al. (2020) for the Milky Way, NGC 253, and NGC 3256, respectively. In the case of NGC 3256, the value is for the southern nucleus. (5) The total SFR. The references are Robitaille & Whitney (2010), Sanders et al. (2003), and Michiyama et al. (2020) for the Milky Way, NGC 253, and NGC 3256, respectively. (6) The 3σ upper limits for high resolution. For NGC 253, we assume 1h. integration assuming 100 mas angular resolution and 10 km s^{-1} spectral resolution (rms=49.7μJy). We assume FWHM=30 km s^{-1} and electron temperature of 4000 K to calculated the 3σ upper limit of SFR. For NGC 3256, we assume 1h. integration assuming 10 mas angular resolution and 10 km s^{-1} spectral resolution (rms=42.3μJy).

vestigate the different modes (i.e., the variation of τ_{gas}) of star formation activities among normal and starburst galaxies. However, the method to measure SFR is also an issue, and measuring τ_{gas} by the same SFR calibration is important to directly compare star formation processes in the Milky Way and active galaxies. Figure 3 is the relation between $\Sigma_{M_{\mathrm{H}_2}}$ and Σ_{SFR} for SgrB2, NGC 253, and NGC 3256 using CO and RRLs, showing $\tau_{\mathrm{gas}} \sim 4$ Gyr in SgrB2, $\tau_{\mathrm{gas}} < 0.1$ Gyr at small clumps in NGC 253, and $\tau_{\mathrm{gas}} \sim 0.1$ Gyr in NGC 3256. This suggests the rapid mode in starbursts and normal mode in SgrB2 although the number of detected clouds are limited. The current important issue in this plot is that the τ_{gas} is measured by different

scales in SgrB2 and NGC 253 and NGC 3256. The ngVLA will detect $1-10$ pc clumps even in NGC 3256 and enable us to understand whether (1) $1-10$ pc scale clumps in the Milky Way and extremely dusty starburst regions in NGC 3256 have same $\tau_{\rm gas}$ or not and (2) the $\tau_{\rm gas}$ of $1-10$ pc clumps are uniform or not in a galaxy (e.g., northern and southern nucleus in NGC 3256).
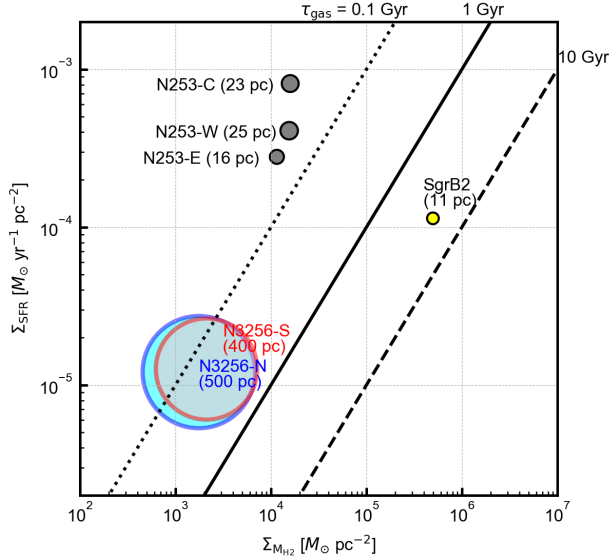

Fig. 3. The relation between $\Sigma_{M_{\rm H2}}$ and $\Sigma_{\rm SFR}$ investigated by RRLs. The yellow circle indicates SgrB2 that has the $\tau_{\rm gas} \sim 4$ Gyr. The grey circles indicates the clumps identified in H40α map in Figure 2(b3) that has $\tau_{\rm gas} \sim 0.02 - 0.04$ Gyr. The red and blue circles indicate the CMZ of merging galaxy NGC 3256 (Michiyama et al. 2020). Current ALMA angular resolution and sensitivity cannot investigate small (a few pc) clumps in NGC 3256. The ngVLA will enable us to investigate small clumps (like SrgB2) even in the intense starburst galaxies such as NGC 3256. For each circle, the size of the markers corresponds to the size of clumps.

4.2. Starburst timescale

The calibration constant between SFR and recombination line luminosity is applicable if SFR is constant over a few Myr. This is because the ionizing photon flux will decrease dramatically after the burst, e.g., by two orders of magnitude between 5-10 Myr (Calzetti et al. 2012). Therefore, recombination lines can measure the "instantaneous" SFR. On the other hand, the calibration constant between SFR and total infrared luminosity ($L_{\rm TIR}$) changes depending on the starburst timescale because old, long lived, low-mass stars contribute TIR luminosity as well as young stellar populations. Therefore, by combining both recombination line and infrared information, we can constrain the starburst time scale. For example, the ratio of SFR measured by recombination lines (SFR$_{\rm RL}$) and $L_{\rm TIR}$ is calculated as

$$\frac{SFR_{\rm RL} \; [M_\odot \; {\rm yr}^{-1}]}{L_{\rm TIR} \; [{\rm erg \; s}^{-1}]} = \begin{cases} 1.6 \times 10^{-44} & (\tau = 10 \; {\rm Gyr}) \\ 2.8 \times 10^{-44} & (\tau = 100 \; {\rm Myr}) \\ 3.7 \times 10^{-44} & (\tau = 10 \; {\rm Myr}) \end{cases} \quad (6)$$

by assuming constant star formation and a Kroupa IMF in the stellar mass range of 0.1–100 $M_\odot$ (Michiyama et al. 2020).

In this analysis, the global RRL luminosity is enough and we do not need to access the spatially resolved maps. Therefore, we can investigate very active galaxies like ULIRGs that is in a relatively distant Universe. Figure 4 shows the expected peak flux of (a) Arp 220 and (b) a ULIRG who has SFR=300 $M_\odot$ yr^{-1} at $z=0.1$. Because a large number of RRLs are populated in ngVLA frequency coverage (Figure 1), stacking methods are also very powerful to detect RRLs from galaxies at a cosmological distance (Emig et al. 2019). The starburst timescale measured by SFR$_{\rm RL}/L_{\rm TIR}$ ratio should be compared with the other timescales such as $\tau_{\rm gas}$ and merger timescale. The detail modeling to convert SFR$_{\rm RL}/L_{\rm TIR}$ to starburst timescale should be developed before the ngVLA era. This goal will be achieved thanks to thr very high sensitivity and wide frequency coverage achieved by ngVLA.
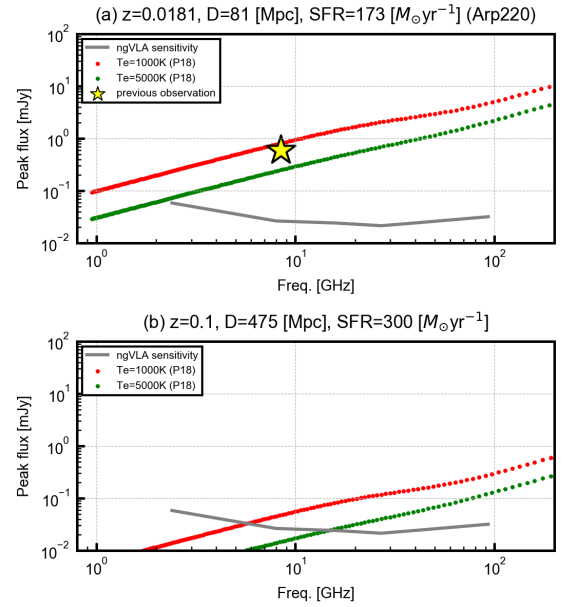

Fig. 4. (a) The red and green dots indicate the expected peak line flux for each RRL assuming $T_{\rm e} = 1000$ K and 5000 K, respectively. The ϵ and $\alpha_{\rm B}$ are calculated by Storey & Hummer (1995) and Prozesky & Smits (2018). The yellow star indicates the previous observation of H92α by VLA (Anantharamaiah et al. 2000). The grey line indicates the naturally weighted ngVLA sensitivity for 1h integration with the velocity resolution of 10 km s^{-1} (https://ngvla.nrao.edu/page/performance). (b) The same plot but we assume a ULIRGs with SFR=300 $M_\odot$ yr^{-1} at $z = 0.1$. The 100 GHz is the most sensitive in this project.

4.3. Properties of H II region

As shown in equation (7), we need to calculate $\alpha_{\rm B}$ and ϵ which depend on $T_{\rm e}$ and $n_{\rm e}$ (Storey & Hummer 1995). The emission flux does not strongly depend on $n_{\rm e}$. However, as shown in Figure (4), the RRL luminosity depends on $T_{\rm e}$. The electron temperature can be estimated by comparing the ratio between RRL and 3 mm continuum flux as follows.

$$R = \frac{\int f_{\nu {\rm RL}} d\upsilon}{f_{\nu {\rm cont}}} \left[\frac{\rm Jy}{\rm Jy \; km \; s^{-1}} \right]$$

$$= 4.38 \times 10^{33} g_{\mathrm{ff}}^{-1} \left[\frac{\epsilon}{\mathrm{erg\ s^{-1}\ cm^{-3}}} \right] \left[\frac{\nu}{\mathrm{GHz}} \right]^{-1} \left[\frac{T_{\mathrm{e}}}{\mathrm{K}} \right]^{0.5} \quad (7)$$

and

$$g_{\mathrm{ff}} = 0.5535 \ln \left| \left[\frac{T_{\mathrm{e}}}{\mathrm{K}} \right]^{1.5} \left[\frac{\nu}{\mathrm{GHz}} \right]^{-1} Z^{-1} \right| - 1.682. \quad (8)$$

Here, we assume an ionic charge of $Z = 1$. We assume that the continuum can be produced by free-free emission from H II regions as well as hydrogen recombination lines. We note that the contribution of dust and synchrotron emissions from supernovae and AGN should be carefully subtracted by continuum SED when we apply this method. The ngVLA's wide frequency enables us to investigate radio continuum SED efficiently. The determination of the electron temperature is one reason why we need both RRL and continuum observations for our purpose. In addition, the electron temperature itself is an important parameter. For example, regions with lower metallicity show higher electron temperature in the Milky Way because the cooling is not efficient in low-metallicity regions (Pagel et al. 1979; Shaver et al. 1983). If the metallicity is measured by the other method, we can investigate whether the relation between metallicity and electron temperature can be reproduced in galaxies.

4.4. Others

Because RRLs are extinction free, the information can be used to investigate the properties of dust by comparing with recombination lines in optical and infrared. For example, the ratio between RRL, Brγ, Brδ, Paα, Paβ, Hα, Hβ represents the dust extinction curve. Based on the absolute extinction magnitude and the slope of the curve, we may investigate the properties of dust (Salim & Narayanan 2020). In addition, we can access the line profile in addition to the total RRL flux. This is an important advantage comparing with the method to measure SFR in continuum observations (for continuum observation, see Murphy et al. 2018). For example, a wing-like structure would be seen both in local ($\sim$pc) and global ($\sim$kpc) scale, which should be important to understand supernovae and AGN feedback processes. Finally, the detection of RRLs in AGN tori is also an important science topics (Izumi et al. 2016).

5. Summary

The ngVLA will provide an unparalleled opportunity for investigating starburst activities at a very dusty nucleus in U/LIRGs by observing RRLs. For example, ngVLA will detect small (1-10 pc) clumps with the SFR of $\sim 0.02\ \mathrm{M_\odot\ yr^{-1}}$ (like SgrB2 of Milky Way) in a merging galaxy NGC 3256 ($D_{\mathrm{L}} \sim 40$ Mpc). This will answer the fundamental question of "whether the star formation process is uniform in normal star forming and extreme starburst galaxies", which will be an important step to answer "How are starbursts triggered and regulated during a galaxy evolution?".

References

Anantharamaiah, K. R., Viallefond, F., Mohan, N. R., Goss, W. M., & Zhao, J. H. 2000, ApJ, 537, 613

Bell, M. B., & Seaquist, E. R. 1977, A&A, 56, 461

Bendo, G. J., Beswick, R. J., D'Cruze, M. J., et al. 2015, MNRAS, 450, L80

Bendo, G. J., Henkel, C., D'Cruze, M. J., et al. 2016, MNRAS, 463, 252

Calzetti, D., Liu, G., & Koda, J. 2012, ApJ, 752, 98

Chaisson, E. J., & Rodriguez, L. F. 1977, ApJL, 214, L111

Daddi, E., Elbaz, D., Walter, F., et al. 2010, ApJL, 714, L118

Emig, K. L., Salas, P., de Gasperin, F., et al. 2019, A&A, 622, A7

Emig, K. L., Bolatto, A. D., Leroy, A. K., et al. 2020, ApJ, 903, 50

Gordon, M. A., & Sorochenko, R. L. 2002, Radio Recombination Lines. Their Physics and Astronomical Applications, Vol. 282, doi:10.1007/978-0-387-09604-9

Immer, K., Schuller, F., Omont, A., & Menten, K. M. 2012, A&A, 537, A121

Izumi, T., Nakanishi, K., Imanishi, M., & Kohno, K. 2016, MNRAS, 459, 3629

Jones, P. A., Burton, M. G., Tothill, N. F. H., & Cunningham, M. R. 2011, MNRAS, 411, 2293

Jones, P. A., Burton, M. G., Cunningham, M. R., et al. 2012, MNRAS, 419, 2961

Kennicutt, R. C., & Evans, N. J. 2012, ARA&A, 50, 531

Madau, P., Ferguson, H. C., Dickinson, M. E., et al. 1996, MNRAS, 283, 1388

Melo, V. P., Pérez García, A. M., Acosta-Pulido, J. A., Muñoz-Tuñón, C., & Rodríguez Espinosa, J. M. 2002, ApJ, 574, 709

Michiyama, T., Iono, D., Nakanishi, K., et al. 2020, ApJ, 895, 85

Mohan, N. R., Goss, W. M., & Anantharamaiah, K. R. 2005, A&A, 432, 1

Murphy, E. J., Condon, J. J., Alberdi, A., et al. 2018, arXiv e-prints, arXiv:1810.07525

Oka, T., Hasegawa, T., Sato, F., Tsuboi, M., & Miyazaki, A. 1998, ApJS, 118, 455

Pagel, B. E. J., Edmunds, M. G., Blackwell, D. E., Chun, M. S., & Smith, G. 1979, MNRAS, 189, 95

Prozesky, A., & Smits, D. P. 2018, MNRAS, 478, 2766

Robitaille, T. P., & Whitney, B. A. 2010, ApJL, 710, L11

Salim, S., & Narayanan, D. 2020, ARA&A, 58, 529

Sanders, D. B., Mazzarella, J. M., Kim, D. C., Surace, J. A., & Soifer, B. T. 2003, AJ, 126, 1607

Seaquist, E. R., & Bell, M. B. 1977, A&A, 60, L1

Shaver, P. A., Churchwell, E., & Rots, A. H. 1977, A&A, 55, 435

Shaver, P. A., McGee, R. X., Newton, L. M., Danks, A. C., & Pottasch, S. R. 1983, MNRAS, 204, 53

Storey, P. J., & Hummer, D. G. 1995, MNRAS, 272, 41

Zavala, J. A., Casey, C. M., Manning, S. M., et al. 2021, arXiv e-prints, arXiv:2101.04734